CHEMISTRY
A EUROPEAN JOURNAL

DOI: 10.1002/chem.200700639

Photoinduced Electron Transfer on Aqueous Carbon Nanohorn–Pyrene–Tetrathiafulvalene Architectures

Georgia Pagona,[a] Atula S. D. Sandanayaka,[b] Alan Maigné,[c] Jing Fan,[c] George C. Papavassiliou,[a] Ioannis D. Petsalakis,[a] Barry R. Steele,[d] Masako Yudasaka,[c] Sumio Iijima,[c] Nikos Tagmatarchis,*[a] and Osamu Ito*[b]

Abstract: Water-soluble carbon-nanohorn–tetrathiafulvalene (CNH-TTF) nanoensembles were prepared by utilizing positively charged pyrene as an assembly medium and characterized by spectroscopy and electron microscopy. Electronic interactions within the nanoensemble were probed by optical spectroscopy, indicating electron transfer between the TTF units and CNHs after light illumination.

Keywords: donor–acceptor systems · electron transfer · nanohorns · radical ions · tetrathiafulvalenes

Introduction

Assembly of individual nanosized molecular building blocks into higher functional materials by advantageous synergistic interactions between each individual part is a fundamental step in nanotechnology.[1] Nanostructured carbon nanohorns (CNHs), a newly discovered and recently mass-produced material,[2] can be used to complement or sometimes alternate with carbon nanotubes en route towards the construction of advanced material architectures with novel properties. Free from any transition-metal contaminants, CNHs self-aggregate forming a secondary spherical superstructure of around 100 nm in diameter.[3] The high porosity and large surface area of CNHs ensure high affinity for organic materials.[4] Furthermore, CNHs hold strong promise both for hydrogen and methane storage,[5] as well as drug delivery systems.[6] However, the insolubility of CNHs in all solvents has to be overcome before considering practical technological applications. Recently, in this context, substantial progress has been made toward solubilization of CNHs. This has been achieved by covalent functionalization of the CNH skeleton[7,8] and highly strained cone-ends[9] as well as through supramolecular π–π stacking interactions[10] with pyrenes and porphyrins.

As the cost of energy and need for energy increases, development of new approaches to harness renewable sources is an important target not only of research interest, but also of practical applications. Converting solar light to electric current through photovoltaic solar cells is nowadays attracting enormous scientific attention as a means of addressing the steadily increasing world's energy requirements.[11] Nature, for billions of years, provides the best paradigm for operating efficient light-driven energy systems. In photosynthesis, solar energy is captured and transferred to the reaction centers, while eventually charge separation for the subsequent electron-transfer process occurs.[12] Electronically excited energies that reach the reaction centers are converted to chemical energy in the form of charge separation across the photosynthetic membrane. In these organized arrays, electrons flow rapidly over long distances with negligible loss of energy. The photosynthesis in plants is a source of inspiration for scientists to engineer non-natural systems that similarly convert light into electrical energy and high chemical potentials. Similar processes occur in artificial pho-

[a] G. Pagona, Dr. G. C. Papavassiliou, Dr. I. D. Petsalakis, Dr. N. Tagmatarchis
Theoretical and Physical Chemistry Institute
National Hellenic Research Foundation
48 Vass. Constantinou Ave., Athens 116 35 (Greece)
Fax: (+30) 210-727-3794
E-mail: tagmatar@eie.gr

[b] A. S. D. Sandanayaka, Prof. O. Ito
Institute of Multidisciplinary Research for Advanced Materials
Tohoku University, Katahira, Aoba-Ku, Sendai, 980–8577 (Japan)
Fax: (+81) 22-217-5608
E-mail: ito@tagen.tohoku.ac.jp

[c] A. Maigné, J. Fan, Dr. M. Yudasaka, Prof. S. Iijima
SORST-JST, Fundamental and Environmental Research Laboratories
NEC Corporation, 34 Miyukigaoka, Tsukuba, Ibaraki 305850 (Japan)

[d] Dr. B. R. Steele
Institute of Organic and Pharmaceutical Chemistry
National Hellenic Research Foundation
48 Vass. Constantinou Ave., Athens 116 35 (Greece)

Supporting information for this article is available on the WWW under http://www.chemeurj.org/ or from the author.

toactive and redox-active molecular donor units linked to acceptors.[13] Such systems are considered as promising for the application in molecular, supramolecular, and nano-electronics. In this context, it is of paramount importance to combine a fast rate for charge separation with a slow rate for charge recombination.

Photoinduced electron-transfer processes in aqueous media are the primary consideration for designing hybrid arrays, in the context of miniature photosynthesis-mimetic systems and photochemical cells for water splitting and reduction of CO_2 to clean fuels.[11] In fact, light-driven hydrogen generation from aqueous systems combined with an electron source represents one of the major challenges in artificial photoconversion devices.[12]

Herein, the preparation, assembly and photophysical studies of a water-soluble nanohybrid consisting of CNHs and an organic π-electron donor, namely tetrathiafulvalene (TTF), are presented. The novelty of the current nanoarchitecture CNH-pyr$^+$-TTF$^-$ relies on the formation of the thermodynamically stable heteroaromatic 1,3-dithiolium cation as well as the gaining of aromaticity upon oxidation of TTF (which is non-aromatic in its ground state).[14] Moreover, an electron-transfer mediator, namely methyl viologen dication (MV^{2+}), as well as a hole-shifting agent such as 1-benzyl-1,4-dihydro-nicotinamide (BNAH), are combined with CNH-pyr$^+$-TTF$^-$ in order to shed light and follow the formation of charge-separated states and subsequent electron-mediating and hole-shifting processes.

Results and Discussion

During the course of the current work, the first carbon-nanotube-based hybrid materials with TTF and extended TTF were recently reported.[15] In our case, the integration of TTF with CNHs was achieved in two steps. Firstly, we capitalized on the high affinity of pyrene chromophores to CNHs, due to π–π stacking interactions.[10a] Thus, we managed to bring CNHs into an aqueous environment upon complexation with a positively charged water-soluble trimethyl(2-oxo-2-pyren-1-yl-ethyl)ammonium bromide (abbreviated as pyr$^+$),[16] forming CNH-pyr$^+$ nanohybrids, stable in water for several months. This procedure, namely the formation of effective π–π stacking interactions between highly planar aromatic compounds with the skeleton of carbon nanotubes (CNTs), is a known and well-established process for dispersing the CNTs in water without significantly altering their novel π-conjugated electronic network.[17] Importantly, the role of pyr$^+$ is dual. Besides aiding on the aqueous solubilization of CNHs, it contributes to the association of and coupling with CNHs negatively charged moieties. Thus, in the second following step, addition of CNH-pyr$^+$ nanohybrids to the lithium salt of 2-(1,3-dithiol-2-ylidine)-1,3-dithiole-4-carboxylate (abbreviated as TTF$^-$),[18] yielded the CNH-pyr$^+$-TTF$^-$ nanoensemble, as shown in Scheme 1.

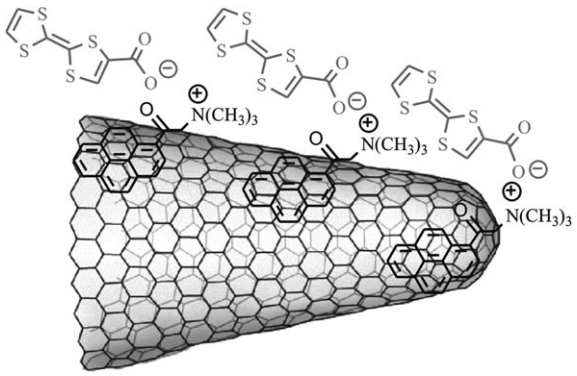

Scheme 1. Partial structure of CNH-pyr$^+$-TTF$^-$ nanoarchitecture.

The immobilization of pyr$^+$ onto CNHs was achieved by simply sonicating and stirring an aqueous solution of pyr$^+$ (10 mL) together with CNHs (1 mg). Excess pyr$^+$ was removed by a series of centrifugation and decantation cycles, which is a purification protocol for CNH-pyr$^+$. Moreover, the latter process minimizes the presence of free pyr$^+$ that would interfere in the following association assays with TTF$^-$.

Electronic absorption spectroscopy was used in the first place to probe the formation of CNH-pyr$^+$ and CNH-pyr$^+$-TTF$^-$ as well as the ground state electronic interactions between the individual components in the nanoensemble. The UV/Vis/NIR spectrum of pristine CNHs exhibits a broad band that monotonically decreases in the NIR region (see Supporting Information, Figure S1). Upon complexation of CNHs with pyr$^+$, the characteristic fine structures due to π–π transitions of pyrene (225, 280, 375, and 405 nm) are collapsed and/or broaden between 230–450 nm, suggesting efficient complexation between the two components (Figure 1a). However, taking into consideration the continuous absorbance of CNHs in the whole UV/Vis/NIR spectrum, it is rather difficult to compare the actual pyr$^+$ concentration in the CNH-pyr$^+$ from the observed absorption intensities. Upon incremental additions (i.e., 100 μL) of CNH-pyr$^+$ to an aqueous solution of TTF$^-$ (10^{-3} mM), the characteristic weak absorptions of TTF$^-$ in the Vis region (400 and 575 nm) broadened and shifted slightly, while a continuous absorbance due to the presence of CNH-pyr$^+$ emerged (Figure 1b). In a blank experiment the electrostatic association of TTF$^-$ with free pyr$^+$ was performed, that is, in the absence of CNHs; only a slight shift and a slight broadening of the sharp bands were observed. Moreover, when pristine CNHs interacted with TTF$^-$, appreciable complexation between the two components was not observed, as derived from the absence of the characteristic absorptions of the TTF$^-$ unit in the electronic absorption spectrum as well as from the insolubility of the CNHs that was retained. All these findings of the electronic absorption spectra, clearly demonstrate that not only the CNH-pyr$^+$-TTF$^-$ nanoensemble is formed, but also, most importantly there is direct π–π electronic communication between the TTF$^-$ π groups with

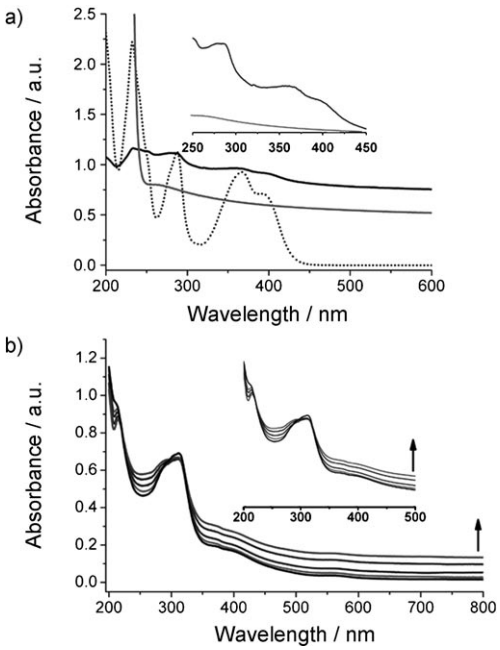

Figure 1. Electronic absorption spectra of a) free pyr$^+$ (dotted line), pristine CNHs (gray) and CNH-pyr$^+$ (black). Inset: an expansion of the 250–450 nm region clearly showing the π–π pyrene transitions; pristine CNHs (gray) and CNH-pyr$^+$ (black). b) Free TTF$^-$ (black) and CNH-pyr$^+$-TTF$^-$ ensemble as formed upon incremental additions of CNH-pyr$^+$ to TTF$^-$, in H_2O (progressive spectra recorded from black to gray).

CNHs in this nanoensemble, in addition to ionic interaction between TTF$^-$ and pyr$^+$ on the CNHs.

ATR-IR spectroscopic studies allowed us to follow the effective electrostatic association between CNH-pyr$^+$ and TTF$^-$ towards the formation of the CNH-pyr$^+$-TTF$^-$ ensemble. As shown in Figure 2, the characteristic carbonyl vibration of the carboxylate unit in TTF$^-$ was shifted from 1704 cm^{-1} for the free lithiated TTF$^-$ to 1673 cm^{-1}—overlapped with the carbonyl unit of the ketone group in the pyr$^+$—upon complexation with the oppositely charged pyr$^+$, while the carbonyl peak in the free pyr$^+$ was also slightly shifted from 1678 cm^{-1} in the CNH-pyr$^+$ complex at 1675 cm^{-1}, thus verifying the formation of the CNH-pyr$^+$-TTF$^-$ nanoensemble. In addition, broadening and decreased intensities of the IR bands may be also suggestive of direct interaction between TTF$^-$ and CNH-pyr$^+$.

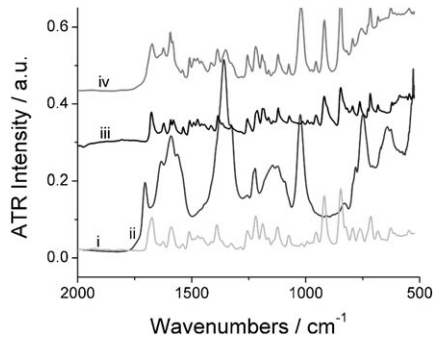

Figure 2. ATR-IR spectra of i) free pyr$^+$, ii) TTF$^-$, iii) CNH-pyr$^+$, and iv) the CNH-pyr$^+$-TTF$^-$ nanoensemble.

Both of the aqueous inklike solutions of CNH-pyr$^+$ and CNH-pyr$^+$-TTF$^-$ were probed by HR-TEM as shown in Figure 3, in which characteristic spherical superstructures of CNHs were visualized, suggesting that the unique morphology of CNHs persisted; that is, conical tips and dahlia flowerlike assemblies with average diameters on the order of 100 nm. Although significant differences between the examined hybrid materials of CNH-pyr$^+$, CNH-pyr$^+$-TTF$^-$ and pristine CNHs are not observed (see Supporting Information, Figure S2), aqueous solubilization of the first two was achieved relative to the insoluble pristine material.

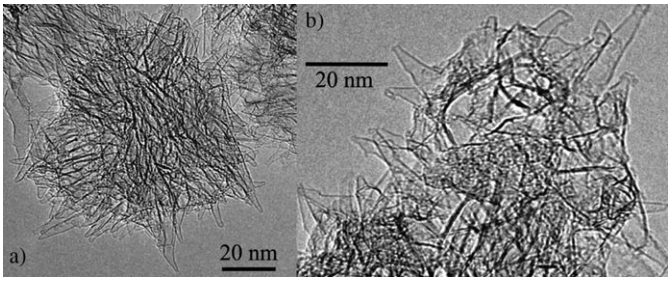

Figure 3. Representative HR-TEM images of a) CNH-pyr$^+$ and b) CNH-pyr$^+$-TTF$^-$ nanoarchitectures.

Energy dispersive X-ray (EDX) spectroscopy is a powerful tool for the elemental investigation of nanohybrids consisting of carbon-rich materials. The EDX spectrum of CNH-pyr$^+$-TTF$^-$ unambiguously identifies the presence of sulfur, demonstrating the integration of the TTF$^-$ unit within the nanoensemble (Figure 4). Further support for the electrostatic complexation of TTF$^-$ to CNH-pyr$^+$ arises from the observation of oxygen in the EDX spectrum of

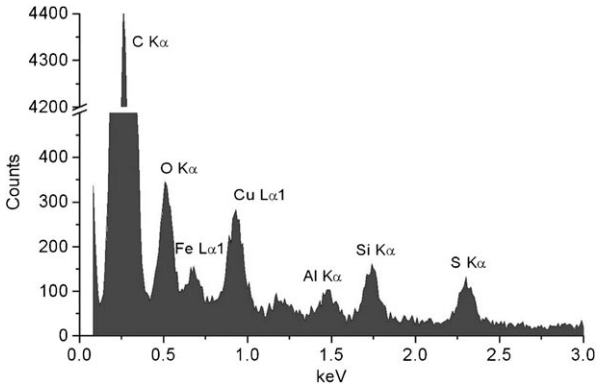

Figure 4. X-ray energy dispersive (EDX) spectrum of CNH-pyr$^+$-TTF$^-$ in which the Kα peak of S at 2.3 keV verifies the presence of TTF in the nanoensemble. The elements Cu, Fe, Al, and Si are detected because of their presence in the microscope equipment, sample holder, and crystal detector.

CNH-pyr$^+$-TTF$^-$ due to presence of carboxylate and ketone groups in TTF$^-$ and pyr$^+$ moieties, respectively.

Raman spectroscopy of pristine CNHs (Figure 5) reveals two characteristic bands, namely, the D- and G-bands, with almost equal strength at 1270 and 1590 cm^{-1}, respectively.[19]

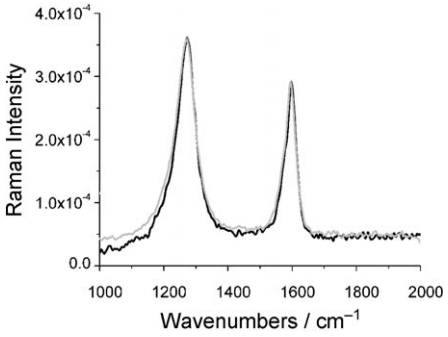

Figure 5. Comparison of normalized Raman spectra of pristine CNHs (light gray), CNH-pyr$^+$ (dark gray), and CNH-pyr$^+$-TTF$^-$ (black), respectively.

The G-band is assigned to the E_{2g}-like vibrations of the sp^2 hybridized carbon network, while the D-band is associated with the A_{1g}-related modes as derived due to the loss of the basal-plane lattice periodicity induced by the conical-shaped tip of CNHs[20] and to sp^3 single-bonding carbon atoms existing within CNHs aggregates.[21] Comparison of the Raman spectra of pristine CNHs with those of CNH-pyr$^+$ and CNH-pyr$^+$-TTF$^-$ demonstrates the noncovalent nature of interactions between the two components as the D/G ratio remains unchanged (Figure 5).

Complementary molecular orbital (MO) calculations, involving geometry optimization at the AM1 level, demonstrated that the physisorbed pyr$^+$ segment lies at about 1.6 Å from the CNHs surface, slightly distorted from planarity (Figure 6). The TTF$^-$ unit recognizes the oppositely charged CNH-pyr$^+$ moiety and lies at approximately 3.5 Å (distance is calculated between the charged atoms forming the nanoensemble). At this level of the MO calculation, the minimum energy of CNH-pyr$^+$-TTF$^-$ is predicted to be more stable compared with the sum of components that form the nanoensemble.

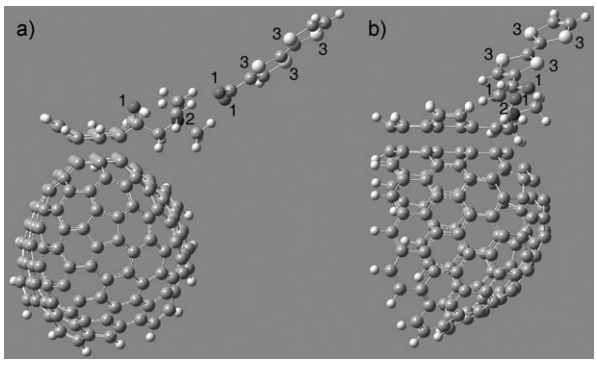

Figure 6. Minimum energy structure of CNH-pyr$^+$-TTF$^-$ nanoensemble resulting from AM1 geometry optimization calculations: a) view along the tip, and b) side view. The numbers 1, 2, and 3 represent oxygen, nitrogen, and sulfur, respectively.

The strong fluorescence emission of pyr$^+$ gave additional advantage to use it as convenient and sensitive probe for intra-ensemble interactions in the CNH-pyr$^+$ hybrid. Similar to recent results obtained on covalently linked pyrenes with CNHs[22] and CNTs,[23] fluorescence peaks of monomeric pyrene with fine structures in the 400–450 nm region and excimer fluorescence in the 450–600 nm region were observed upon excitation at 360 nm. From the comparison of intensities intrahybrid fluorescence quenching occurs in the CNH-pyr$^+$ hybrid as shown in Figure 7. Evidently, the effective

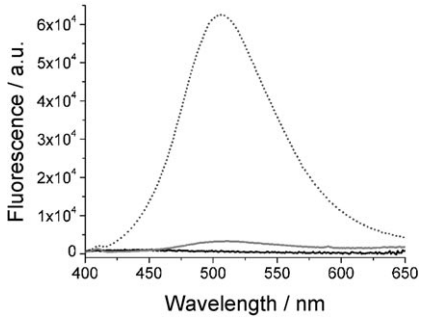

Figure 7. Steady-state fluorescence spectra of CNH-pyr$^+$-TTF$^-$ (black), CNH-pyr$^+$ (gray) and pyr$^+$ (dotted), as obtained in aqueous samples displaying matching absorbances at the excitation wavelength ($\lambda_{exc.}$ = 360 nm).

quenching of CNH-pyr$^+$ fluorescence suggests stronger interaction of pyrene with CNHs. Additionally, further quenching of the pyr$^+$ fluorescence was observed in the CNH-pyr$^+$-TTF$^-$ nanoensemble, verifying the importance of the attractive electrostatic interactions between pyr$^+$ and TTF$^-$ in the CNH-pyr$^+$-TTF$^-$ nanoensemble.

At this point it should be emphasized that additional control experiments were carried out in order to verify the above results, that is, simply associating TTF$^-$ with pyr$^+$ through coulombic interactions (i.e. in the absence of CNHs) gave no significant changes in the fluorescence intensity of the free pyr$^+$. Additionally, no change in the fluorescence spectra was observed when we attempted the interaction of neutral TTF with the CNH-pyr$^+$ nanohybrid, verifying the importance of the synergistic electrostatic interactions for the realization of the CNH-pyr$^+$-TTF$^-$ nanoensemble, although this observation does not always exclude the possible association of TTF with the surface CNHs.

To further support our results and get additional insights on the electronic communication between individual parts within the assembled hybrid system, time-resolved fluorescence and transient absorption studies were undertaken. The fluorescence spectra observed with a streak-scope are shown in the inset of Figure 8, in which the spectral area of pyr$^+$ is almost normalized. The broadening of the fluorescence spectral bandwidth was observed between CNHs and

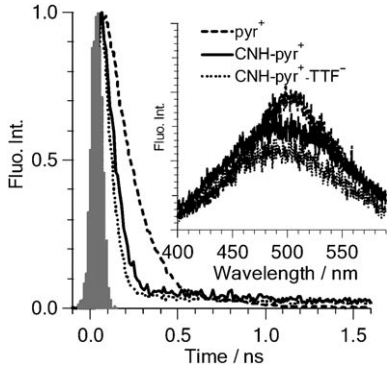

Figure 8. Fluorescence decay profiles of aqueous solutions of pyr^+ in comparison with CNH-pyr^+ and CNH-pyr^+-TTF^- nanoensembles, respectively, in aqueous solution. Inset: Time-resolved fluorescence spectra.

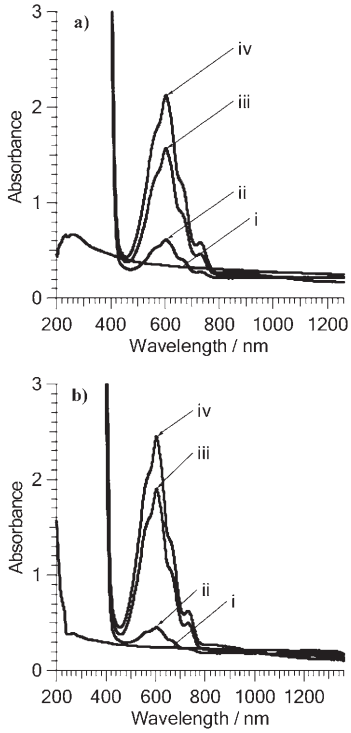

Figure 9. Steady-state electronic absorption spectra of a) CNH-pyr^+ and b) CNH-pyr^+-TTF^- nanoensembles, in the presence of 5 mM MV^{2+} and i) 0 mM BNAH, ii) 1 mM BNAH, iii) 3 mM BNAH, and iv) 5 mM BNAH, observed during repeated 355 nm laser light (6 ns, 6 mJ) irradiation in Ar-saturated aqueous solution.

pyr^+; furthermore, this trend was slightly increasing for spectrum between TTF^- and pyr^+ on the CNH surface. The fluorescence time profiles in Figure 8 indicate that the pyr^+ emission was efficiently quenched by nanohorns in the CNH-pyr^+ nanohybrid. The fluorescence decay lifetime, calculated to be 83 ps, is shorter than the 178 ps of unbound pyr^+, which was rationalized by appreciable interaction of pyr^+ with the surface of the nanohorn, allowing sufficient coverage of the CNHs surface with pyr^+ units. The latter is responsible for the observed efficient charge separation within this nanosystem. Further shortening (66 ps) was observed upon integration of TTF^- in CNH-pyr^+-TTF^-, suggesting additional interaction between TTF^- and pyr^+ on the CNH surface. The most probable interpretation of this behavior is an increase in the donor ability of the excited singlet state of pyr^+ in combination with TTF^-, which reduces the electron-withdrawing ability of the ammonium cation connected to the pyrene unit.

To shed light on the process after the photoexcitation of CNH-pyr^+ and CNH-pyr^+-TTF^-, steady-state absorption measurements were conducted upon addition of methyl viologen dication (MV^{2+}) and 1-benzyl-1,4-dihydronicotinamide (BNAH), as electron mediator and hole-shifter, respectively. Importantly, during photolysis at 355 nm, accumulation of $MV^{\bullet+}$ was observed for both CNH-pyr^+ and CNH-pyr^+-TTF^- nanohybrids as shown in Figure 9. In combination with the fluorescence quenching of pyr^+ in CNH-pyr^+, the charge-separation takes place from the singlet excited state of pyr^+ to CNHs, generating a hole in the π system of pyr^+ and an electron in CNHs; this electron then moves to MV^{2+}. In the presence of BNAH, a hole in pyr^+ shifts to sacrificial BNAH; this results in the retardation of the charge-recombination and, hence, persistent $MV^{\bullet+}$. Increase of the BNAH concentration enhances the maximum $MV^{\bullet+}$ concentration, indicating that the hole-shifting reagent indeed assists the accumulation of $MV^{\bullet+}$ (Figure 9), retarding the charge recombination processes. Moreover, in CNH-pyr^+-TTF^-, additional $MV^{\bullet+}$ was accumulated, suggesting the increase in the charge-separation, in accord with the higher fluorescence quenching. Importantly, in controlled experiments without CNHs such $MV^{\bullet+}$ accumulation was not observed. However, it cannot be excluded that direct excitation of the TTF^- moiety assists the generation of $MV^{\bullet+}$.

At this point, for which the charge-separation through the excited state of pyr^+ is examined, the rate (k_{CS}) and quantum yield for the charge-separation generating $(CNH)^{\bullet-}$-$(pyr^+)^{\bullet+}$ were evaluated from the fluorescence lifetimes of pyr^+ as $6.4\times10^9\ s^{-1}$ and 0.53, respectively. In the supramolecular ensemble formation upon integration of TTF^-, further acceleration of the charge-separation was revealed by the shortening of the fluorescence lifetimes, from which the rate and quantum yield for the charge-separation generating $(CNH)^{\bullet-}$-$(pyr^+)^{\bullet+}$-TTF^- and/or $(CNH)^{\bullet-}$-pyr^+-$(TTF^-)^{\bullet+}$ were evaluated to be $9.5\times10^9\ s^{-1}$ and 0.63, respectively.

In additional experiments utilizing 532 nm laser light, which excites predominantly the CNHs, similar accumulation of $MV^{\bullet+}$ was observed, although the maximum $MV^{\bullet+}$ concentration was lower than the one observed with 355 nm laser light excitation. This finding nicely demonstrates that direct excitation of CNHs may also generate the charge-separated state in the presence of the pyr^+ and pyr^+-TTF^- moieties as electron donors, although the efficiencies are lower than those with 355 nm laser light, which excites the pyr^+ and TTF^- moieties in addition to CNHs.

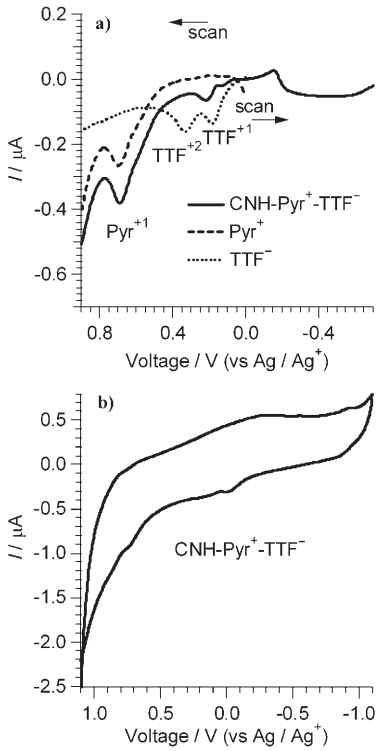

Figure 10. a) Differential pulse voltammograms of CNH-pyr$^+$-TTF$^-$ and references. b) Cyclic voltammogram of CNH-pyr$^+$-TTF$^-$ in deaerated H_2O with a scan rate of 100 mV s^{-1}.

The electrochemistry of CNH-pyr$^+$-TTF$^-$ was investigated by differential pulse voltammetry (DPV) as well as cyclic voltammetry (CV). The measurements were performed in deaerated distilled water containing 0.10 M KCl as a supporting electrolyte with a scan rate of 100 mV s^{-1}, a glassy carbon working electrode and a Pt counter electrode. The measured potentials were recorded with Ag/AgCl (saturated KCl) as a reference electrode. The voltammograms revealed a continuum of diffusion controlled cathodic current, namely, progressive filling of empty low-energy manifold orbitals of CNHs or emptying of the occupied electronic states of pyr$^+$, TTF$^-$, and CNHs. This observation is in line with previous reports of porphyrin-functionalized CNHs[8b] as well as with the first report of covalently associated TTF to carbon nanotubes.[14] As shown in Figure 10, DPV and CV measurements revealed:

1) The oxidation potential of pyr$^+$ in CNH-pyr$^+$-TTF$^-$ found at 0.65 V vs Ag/AgCl anodically shifted by approximately 90 mV relative to the reference of pyr$^+$. This anodic shift implies considerable electronic interactions in the CNH-pyr$^+$ hybrid, as also proved by UV/Vis and fluorescence spectroscopy, which render easier the oxidation of pyr$^+$.
2) Two one-electron reversible oxidation processes of TTF$^-$ at 0.22 V and 0.13 V anodically shifted by 120 mV and 90 mV, respectively, relative to free TTF$^-$.
3) The voltage onset observed at −0.25 V is attributed to the limiting reduction potential of CNHs.

The possible charge-separation processes can be supported with the these electrochemical data; the free energy of the charge-separation through the excited state of pyr$^+$ (2.5 eV from 500 nm fluorescence) can be evaluated by the oxidation potentials of pyr$^+$ (0.56 V vs. Ag/AgCl) and reduction potential of CNHs (−0.25 V vs. Ag/AgCl) to be −1.6 eV for (CNH)$^{\bullet-}$-(pyr$^+$)$^{\bullet+}$-TTF$^-$. Thus, this process would be exothermic through the excited singlet state of pyr$^+$. The energy of (CNH)$^{\bullet-}$-pyr$^+$-(TTF$^-$)$^{\bullet+}$ from the ground state is approximately −0.4 eV, which is less negative than the value (0.81 eV) of (CNH)$^{\bullet-}$-(pyr$^+$)$^{\bullet+}$-TTF$^-$, although these values depend on the distance. Thus, hole shift from (pyr$^+$)$^{\bullet+}$ to TTF$^-$ would be anticipated to occur.

Transient absorption measurements were also carried out. Broad absorption bands, upon 355 nm laser light excitation of CNH-pyr$^+$-TTF$^-$ were observed in the Vis/NIR regions and found to decay within 100 ns (Figure 11). The radical

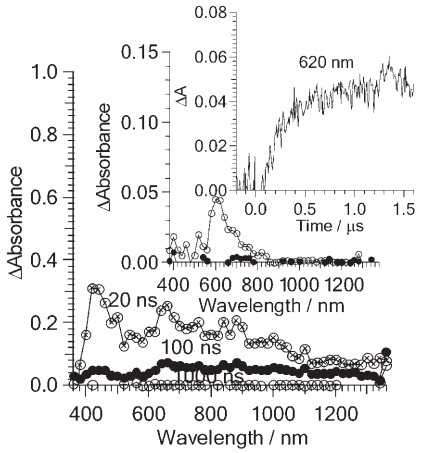

Figure 11. Transient absorption spectra of CNH-pyr$^+$-TTF$^-$ as observed at 355 nm laser light excitation. Insets: Transient absorption spectra of CNH-pyr$^+$-TTF$^-$ in the presence of 5 mM MV^{2+} and 5 mM BNAH and time profile at 620 nm in Ar-saturated aqueous solution.

cation of the pyrene substituted by a carbonyl group has absorption peaks at 500 nm with weak absorption in the longer wavelength as observed for CNH-pyr$^+$ (see Supporting Information, Figure S3).[24] In addition, the broad absorption bands in the 600–1000 nm region in Figure 11 can be attributed to the radical cation of TTF moiety.[25] It is reasonable to ascribe the remaining absorption bands longer than 1000 nm to the trapped electron on the CNHs. Therefore, the transient spectra gave an evidence to support the generations of the charge-separated states such as (CNH)$^{\bullet-}$-pyr$^+$-(TTF$^-$)$^{\bullet+}$ and (CNH)$^{\bullet-}$-(pyr$^+$)$^{\bullet+}$-TTF$^-$. The decay time profiles for these transient species gave the charge-recombination rate (k_{CR}) to be 1.5×10^7 s^{-1} (see Supporting Information, Figure S4), from which the lifetime of the charge-separated state can be evaluated to be about 70 ns, which may

be mainly attributed to long-lived $(CNH)^{\bullet-}$-pyr^{+}-$(TTF^{-})^{\bullet+}$ rather than short-lived $(CNH)^{\bullet-}$-$(pyr^{+})^{\bullet+}$-TTF^{-}. Upon addition of MV^{2+} and BNAH, the transient absorption almost disappeared leaving the characteristic absorption of $MV^{\bullet+}$ at 620 nm (inset Figure 11), which supports the electron migration from the electron-rich species, such as $(CNH)^{\bullet-}$ in $(CNH)^{\bullet-}$-pyr^{+}-$(TTF^{-})^{\bullet+}$ and $(CNH)^{\bullet-}$-$(pyr^{+})^{\bullet+}$-TTF^{-}. The rise time profile at 620 nm corresponds to the intermolecular electron-mediating rate constant ($1.0\times10^{10}\,M^{-1}\,s^{-1}$) from $(CNH)^{\bullet-}$ to MV^{2+}. Since the ratio of k_{CS}/k_{CR} is higher than 500, the chance of electron migration from $(CNH)^{\bullet-}$ to MV^{2+} with a diffusion controlled limit in D_2O is highly possible. These processes are summarized in Scheme 2a.

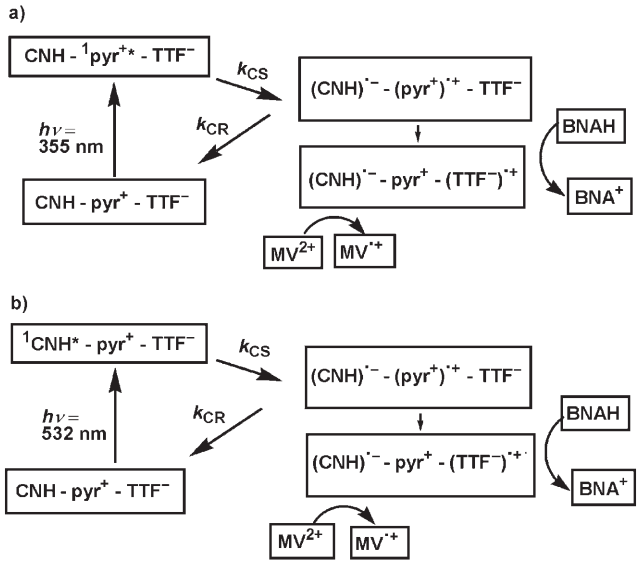

Scheme 2. Photoinduced processes initiated by a) pyr^{+} excitation and b) CNHs excitation; BNA^{+} refers as to 1-benzyl-nicotinamide cation.

Photoexcitation of CNHs was also found to effect the $MV^{\bullet+}$ generation, most likely because the charge-separation takes place through the excited state of CNHs as shown in Scheme 2b. Another possibility is direct charge-separation from CNHs to MV^{2+}. These all mechanisms cooperatively contribute to the $MV^{\bullet+}$ accumulation as a whole. This phenomenon is quite important for wide carbon-nanotechnological application in terms of solar light and energy-conversion systems. For example, the $MV^{\bullet+}$ generation under visible-light irradiation of water soluble CNHs may open the way to hydrogen evolution by solar light and reduction of CO_2 to fuels in the presence of appropriate metal catalysts.

Conclusion

Coulombic association of negatively charged tetrathiafulvalene carboxylate (TTF^{-}) units with positively charged pyrene (pyr^{+}) noncovalently associated on the surface of CNHs allowed dissolution of the nanosized CNH-pyr^{+}-TTF^{-} architecture in aqueous environment. A complete spectroscopic characterization of CNH-pyr^{+}-TTF^{-}, complemented with electron microscopy analysis and MO calculations, was performed. The one-electron reduced and oxidized species such as $(CNH)^{\bullet-}$-pyr^{+}-$(TTF^{-})^{\bullet+}$ and $(CNH)^{\bullet-}$-$(pyr^{+})^{\bullet+}$-TTF^{-} were identified directly by the transient spectral measurements and indirectly by the accumulation of electron on methyl viologen dication (MV^{2+}), giving the radical monocation ($MV^{\bullet+}$). Kinetic analyses of the time profiles of the fluorescence and transient absorptions gave information regarding charge-separation rate and quantum yields through the excited singlet sate of pyr^{+} and lifetimes for the charge-separated state, respectively. In addition, the photoexcitation of CNHs also afforded the accumulation of $MV^{\bullet+}$, suggesting the photoinduced charge-separation through the CNHs.

Experimental Section

All solvents and reagents were purchased from Aldrich and were used without further purification. All experiments were performed at room temperature. The pyr^{+} and TTF^{-} were synthesized according to published procedures.[16,18] The preparation of water-soluble CNH-pyr^{+} was achieved by adding pristine CNHs (1 mg) to an aqueous solution of pyr^{+} (10^{-5} M, 5 mL). The mixture was sonicated for 5 min and then stirred at room temperature for 18 h. After that period, it was centrifuged and the dark-yellow supernatant layer containing free pyr^{+} in solution was decanted. Distilled water was added to the black solid residue, which was re-suspended by sonication for 30 s. The same cycle, namely centrifugation-decantation-suspension was repeated twice to remove completely the unbound pyr^{+}.

HR-TEM measurements were carried out on a 002B Topcon operated at an accelerating voltage of 120 kV for imaging. EDX analysis was performed on the same HR-TEM instrument equipped with an X-ray detector (5538 A-4SUS-SN, Thermo Electron Inc.). Mid-infrared spectra in the region 550–4000 cm^{-1} were obtained on a Fourier Transform IR spectrometer (Equinox 55 from Bruker Optics) equipped with a single reflection diamond ATR accessory (DuraSamp1IR II by SensIR Technologies). Steady state UV/Vis electronic absorption spectra were recorded on a Perkin Elmer (Lambda 19) UV/Vis/NIR spectrophotometer. The Raman spectra were measured on a Fourier transform instrument (RFS 100 Bruker Optics) employing about 360 mW of the Nd-YAG 1064 nm line in a backscattering geometry. Steady-state emission spectra were recorded with a Fluorolog-3 Jobin Yvon-Spex spectrofluorometer (model GL3–21). The picosecond time-resolved fluorescence spectra were measured using an argon-ion pumped Ti:sapphire laser (Tsunami) and a streak scope (Hamamatsu Photonics). Nanosecond transient absorption spectra in the visible and NIR regions were measured by means of laser-flash photolysis; 355 and 532 nm light from a Nd:YAG laser were used as the exciting source and Ge-avalanche-photodiode modules were used for detecting the monitoring light from a pulsed Xe lamp.

Acknowledgements

This work, conducted as part of the award "Functionalization of Carbon Nanotubes Encapsulating Novel Carbon-based Nanostructured Materials" made under the European Heads of Research Councils and European Science Foundation EURYI (European Young Investigator) Awards scheme, was supported by funds from the Participating Organizations of EURYI and the EC Sixth Framework Programme. Experimental assistance of Dr. Theodoros Felekis is acknowledged. The present work was

supported by the Ministry of Education, Culture, Sports, Science and Technology of Japan by a Grants-in-Aid on Scientific Research on Priority Areas (417).

[1] a) *Introduction to Nanotechnology* (Eds.: C. P. Poole, F. J. Owens), Wiley-VCH, Weinheim, **2003**; b) *Nanophysics and Nanotechnology: An Introduction to Modern Concepts in Nanoscience* (Ed.: E. L. Wolf), Wiley, New York, **2004**.

[2] a) S. Iijima, M. Yudasaka, R. Yamada, S. Bandow, K. Suenaga, F. Kokai, K. Takahashi, *Chem. Phys. Lett.* **1999**, *309*, 165; b) S. Bandow, F. Kokai, K. Takahashi, M. Yudasaka, L. C. Qin, S. Iijima, *Chem. Phys. Lett.* **2000**, *321*, 514; c) J. A. Nisha, M. Yudasaka, S. Bandow, F. Kokai, K. Takahashi, S. Iijima, *Chem. Phys. Lett.* **2000**, *328*, 321; d) K. Murata, K. Kaneko, F. Kokai, K. Takahashi, M. Yudasaka, S. Iijima, *Chem. Phys. Lett.* **2000**, *331*, 14; e) S. Iijima, *Physica B* **2002**, *323*, 1.

[3] D. Kasuya, M. Yudasaka, K. Takahashi, F. Kokai, S. Iijima, *J. Phys. Chem. B* **2002**, *106*, 4947.

[4] a) J. Fan, M. Yudasaka, Y. Kasuya, D. Kasuya, S. Iijima, *Chem. Phys. Lett.* **2004**, *397*, 5; b) R. Yuge, M. Yudasaka, J. Miyawaki, Y. Kubo, T. Ichihashi, H. Imai, E. Nakamura, H. Isobe, H. Yorimitsu, S. Iijima, *J. Phys. Chem. B* **2005**, *109*, 178861.

[5] a) K. Murata, K. Kaneko, H. Kanoh, D. Kasuya, K. Takahashi, F. Kokai, M. Yudasaka, S. Iijima, *J. Phys. Chem. B* **2002**, *106*, 11132; b) H. Tanaka, H. Kanoh, M. El-Merraoui, W. A. Steele, M. Yudasaka, S. Iijima, K. Kaneko, *J. Phys. Chem. B* **2004**, *108*, 17457; c) E. Bekyarova, K. Murata, M. Yudasaka, D. Kasuya, S. Iijima, H. Tanaka, H. Kahoh, K. Kaneko, *J. Phys. Chem. B* **2003**, *107*, 4681; d) K. Murata, A. Hashimoto, M. Yudasaka, D. Kasuya, K. Kaneko, S. Iijima, *Adv. Mater.* **2004**, *16*, 1520.

[6] H. Murakami, K. Ajima, J. Miyawaki, M. Yudasaka, S. Iijima, K. Shiba, *Mol. Pharm.* **2004**, *1*, 399.

[7] a) N. Tagmatarchis, A. Maigne, M. Yudasaka, S. Iijima, *Small* **2006**, *2*, 490; b) G. Pagona, A. S. D. Sandanayaka, Y. Araki, J. Fan, N. Tagmatarchis, G. Charalambidis, A. G. Coutsolelos, B. Boitrel, M. Yudasaka, S. Iijima, O. Ito, *Adv. Funct. Mater.* **2007**, *17*, 1705.

[8] a) C. Cioffi, S. Campidelli, F. G. Brunetti, M. Meneghetti, M. Prato, *Chem. Commun.* **2006**, 2129; b) C. Cioffi, S. Campidelli, C. Sooambar, M. Marcaccio, G. Marcolongo, M. Meneghetti, D. Paolucci, F. Paolucci, G. Ehli, G. M. Aminur Rahman, V. Sgobba, D. M. Guldi, M. Prato, *J. Am. Chem. Soc.* **2007**, *129*, 3938.

[9] G. Pagona, J. Fan, N. Tagmatarchis, M. Yudasaka, S. Iijima, *Chem. Mater.* **2006**, *18*, 3918.

[10] a) J. Zhu, D. Kase, K. Shiba, D. Kasuya, M. Yudasaka, S. Iijima, *Nanolett.* **2003**, *3*, 1033; b) G. Pagona, A. S. D. Sandanayaka, Y. Araki, J. Fan, N. Tagmatarchis, M. Yudasaka, S. Iijima, O. Ito, *J. Phys. Chem. B* **2006**, *110*, 20729; c) G. Pagona, J. Fan, A. Maigne, M. Yudasaka, S. Iijima, N. Tagmatarchis, *Diamond Relat. Mater.* **2007**, *16*, 1150.

[11] a) *Photochemical Conversion and Storage of Solar Energy* (Eds.: E. Pelizzetti, M. Schiavello), Kluwer, Dordrecht, **1997**; b) *Electron Transfer in Chemistry* (Ed.: V. Balzani), Wiley-VCH, Weinheim, **2001**.

[12] *Solar Energy Conversion* (Eds.: E. Grätzel, J.-E. Moser), Wiley-VCH, Weinheim, **2001**.

[13] a) *Artificial Photosynthesis: From Basic Biology to Industrial Application* (Eds.: A. F. Collings, C. Critchley), Wiley-VCH, Weinheim, **2005**; b) D. Gust, T. A. Moore, A. L. Moore, *Acc. Chem. Res.* **1993**, *26*, 198; c) N. Martin, L. Sanchez, B. Illescas, I. Perez, *Chem. Rev.* **1998**, *98*, 2527; d) H. Imahori, Y. Sakata, *Eur. J. Org. Chem.* **1999**, 2445; e) D. Gust, T. A. Moore, A. L. Moore, *Acc. Chem. Res.* **2001**, *34*, 40; f) D. M. Guldi, *Chem. Soc. Rev.* **2002**, *31*, 22; g) H. Imahori, Y. Mori, Y. Matano, *J. Photochem. Photobiol. C* **2003**, *4*, 51; h) S. Fukuzumi, *Org. Biomol. Chem.* **2003**, *1*, 609; i) S. Fukuzumi, K. Ohkubo, H. Imahori, D. M. Guldi, *Chem. Eur. J.* **2003**, *9*, 1585; j) J. L. Segura, N. Martin, D. M. Guldi, *Chem. Soc. Rev.* **2005**, *34*, 31; k) D. M. Guldi, G. M. A. Rahman, V. Sgobba, C. Ehli, *Chem. Soc. Rev.* **2006**, *35*, 471; l) D. M. Guldi, *Phys. Chem. Chem. Phys.* **2007**, *9*, 4000; m) P. V. Kamat, *J. Phys. Chem. C* **2007**, *111*, 2834.

[14] a) N. Martín, L. Sanchez, D. M. Guldi, *Chem. Commun.* **2000**, 113; b) N. Martín, L. Sanchez, B. Illescas, S. Gonzalez, M. A. Herranz, D. M. Guldi, *Carbon* **2000**, *38*, 1577; c) N. Martín, L. Sanchez, M. A. Herranz, D. M. Guldi, *J. Phys. Chem. A* **2000**, *104*, 4648; d) D. M. Guldi, S. Gonzalez, N. Martín, A. Anton, J. Garyn, J. Orduna, *J. Org. Chem.* **2000**, *65*, 1978; e) S. Gonzalez, A. Swartz, N. Martín, D. M. Guldi, *Org. Lett.* **2003**, *5*, 557.

[15] M. Angeles Herranz, N. Martin, S. Campidelli, M. Prato, G. Brehm, D. M. Guldi, *Angew. Chem.* **2006**, *118*, 4590; *Angew. Chem. Int. Ed.* **2006**, *45*, 4478; .

[16] N. Nakashima, Y. Tomonari, H. Murakami, *Chem. Lett.* **2002**, 638.

[17] a) R. J. Chen, Y. Zhang, D. Wang, H. Dai, *J. Am. Chem. Soc.* **2001**, *123*, 3838; b) H. Murakami, T. Nomura, N. Nakashima, *Chem. Phys. Lett.* **2003**, *378*, 481; c) H. Li, B. Zhou, Y. Lin, L. Gu, W. Wamg, K. A. S. Fernando, S. Kumar, L. F. Allard, Y. -P. Sun, *J. Am. Chem. Soc.* **2004**, *126*, 1014; d) D. M. Guldi, G. M. A. Rahman, N. Tagmatarchis, M. Prato, *Angew. Chem.* **2004**, *116*, 5642; *Angew. Chem. Int. Ed.* **2004**, *43*, 5526; ; e) J. Chen, C. P. Collier, *J. Phys. Chem. B* **2005**, *109*, 7605; f) T. Hasobe, S. Fukuzumi, P. V. Kamat, *J. Am. Chem. Soc.* **2005**, *127*, 11884; g) D. M. Guldi, G. M. Aminur Rahman, N. Jux, D. Balbinot, U. Hartnagel, N. Tagmatarchis, M. Prato, *J. Am. Chem. Soc.* **2005**, *127*, 9830; h) D. M. Guldi, G. M. A. Rahman, N. Jux, D. Balbinot, N. Tagmatarchis, M. Prato, *Chem. Commun.* **2005**, 2038; i) G. Ehli, G. M. Aminur Rahman, N. Jux, D. Balbinot, D. M. Guldi, F. Paolucci, M. Marcaccio, D. Paolucci, M. Melle-Franco, F. Zerbetto, S. Campidelli, M. Prato, *J. Am. Chem. Soc.* **2006**, *128*, 11222.

[18] J. Garin, J. Orduna, S. Uriel, A. J. Moore, M. R. Bryce, S. Wegener, D. S. Yufit, J. A. K. Howard, *Synthesis* **1994**, 489.

[19] T. Yamaguchi, S. Bandow, S. Iijima, *Chem. Phys. Lett.* **2004**, *389*, 181.

[20] a) A. M. Rao, E. Richter, S. Bandow, B. Chase, E. C. Eklund, K. A. Williams, S. Fang, K. R. Subbaswamy, M. Menon, A. Thess, R. E. Smalley, G. Dresselhaus, M. S. Dresselhaus, *Science* **1997**, *275*, 187; b) S. Iijima, T. Ichihashi, Y. Ando, *Nature* **1992**, *356*, 776; c) F. Tuinstra, J. L. Koenig, *J. Compos. Mater.* **1970**, *4*, 492.

[21] S. Utsumi, H. Honda, Y. Hattori, H. Kanoh, K. Takahashi, H. Sakai, M. Abe, M. Yudasaka, S. Iijima, K. Kaneko, *J. Phys. Chem. C* **2007**, *111*, 5572.

[22] A. S. D. Sandanayaka, G. Pagona, N. Tagmatarchis, M. Yudasaka, S. Iijima, Y. Araki, O. Ito, *J. Mater. Chem.* **2007**, *17*, 2540.

[23] a) L. Qu, R. B. Martin, W. Huang, K. Fu, D. Zweifel, Y. Lin, Y. -P. Sun, C. E. Bunker, B. A. Harruff, J. R. Gord, L. F. Allard, *J. Chem. Phys.* **2002**, *117*, 8089; b) R. B. Martin, L. Qu, Y. Li, B. A. Harruff, C. E. Bunker, J. R. Gord, L. F. Allard and Y. -P. Sun, *J. Phys. Chem. B* **2004**, *108*, 11447.

[24] C. Ehli, G. M. A. Rahman, N. Jux, D. Balbinot, D. M. Guldi, F. Paolucci, M. Marcaccio, D. Paolucci, M. Melle-Franco, F. Zerbetto, S. Campidelli, M. Prato, *J. Am. Chem. Soc.* **2006**, *128*, 11222.

[25] N. Martin, L. Sanchez, M. A. Herranz, D. M. Guldi, *J. Phys. Chem. A* **2000**, *104*, 4648.

Received: April 26, 2007
Published online: August 3, 2007

